



## Detecting tsunami-induced damage on building side walls using X-band of post-event airborne full polarimetric SAR data

H. Gokon<sup>(1)</sup>, M. Jimbo<sup>(2)</sup>, S. Koshimura<sup>(3)</sup>, C.N. Koyama<sup>(4)</sup>, M. Sato<sup>(5)</sup> and K. Meguro<sup>(6)</sup>

<sup>(1)</sup> Research associate, Institute of industrial science, The University of Tokyo, Japan, gokon@iis.u-tokyo.ac.jp

<sup>(2)</sup> Company worker who graduated Tohoku University, Oki data corporation, Japan jimbo@geoinfo.civil.tohoku.ac.jp

<sup>(3)</sup> Professor, International Research Institute of Disaster Science (IRIDeS), Tohoku University, koshimura@irides.tohoku.ac.jp

<sup>(4)</sup> Postdoctoral researcher, Center for Northeast Asian Studies (CNEAS), Tohoku University, christian.koyama@cneas.tohoku.ac.jp

<sup>(5)</sup> Professor, Center for Northeast Asian Studies (CNEAS), Tohoku University, sato@cneas.tohoku.ac.jp

<sup>(6)</sup> Professor, Institute of industrial science, The University of Tokyo, Japan, meguro@iis.u-tokyo.ac.jp

### Abstract

A new method for detecting tsunami-induced damage on a building side wall is proposed using X-band of post-event full polarimetric airborne synthetic aperture radar (Pi-SAR2) data. Buildings with destroyed walls are distinguished based on the ratio of the double-bounce scattering power to the total scattering power in the building layover areas. A building side wall shows bright backscattering induced by layover and double-bounce scattering. If the lower part of a building side wall is destroyed by a tsunami, double-bounce scattering, which is dominant in the lower part of the wall, may be absent and its scattering power may decrease. Considering the radar properties in terms of building side walls, a method for distinguishing destroyed building side walls was developed using post-event full polarimetric SAR (PolSAR) data. A four-component decomposition model and the Yamaguchi four-component decomposition scheme were applied to compute the double-bounce scattering power using polarimetric SAR data. The ratio of the double-bounce scattering power to the total scattering power in the layover area was estimated and correlated with the surveyed data. A classifier for damage detection was created using this data set. To create the classifier, a decision tree application of a machine learning algorithm was applied, which discriminates between “destroyed” and “undestroyed” building side walls. The developed classifier was validated using 12 buildings with 48 side walls and demonstrated satisfactory performance with 77.1 % accuracy and a kappa statistic of 0.48.

*Keywords: tsunami, remote sensing, SAR, building damage*

## 1. Introduction

On March 11, 2011, a 9.0 Mw earthquake and subsequent tsunami occurred along the coastal areas of the Tohoku region of Japan. The tsunami produced a maximum run-up height of 40.1 m; caused major damage to buildings, forests, and infrastructure; and eroded the coastline [1]. As of August 10, 2014, Japan's National Police Agency reported a total of 18,499 fatalities or missing persons and 127,390 buildings and/or houses that collapsed or were washed away by the tsunami [2]. Since the 2011 Tohoku earthquake and tsunami, the characteristics of the tsunami and its impacts have been investigated using several approaches, such as field surveys, numerical modeling and remote sensing technology [3].

Each approach has advantages and disadvantages; therefore, an optimal approach should be selected based on the required information. Remote sensing technology is useful for assessing extensive damage. Synthetic aperture radar (SAR), which functions quasi regardless of weather or daylight conditions, is powerful for rapid observations of an affected area [4].

Methods for detecting building damage resulting from natural disasters have been developed in recent decades ([5], [6]). After the launch of TerraSAR-X(DLR) and CosmoSkyMed, which are equipped with high-resolution active sensors, in 2007, approaches based on a building unit scale that consider high-resolution SAR data have been increasingly proposed ([7], [8]). In the case of the 2011 Tohoku event, airborne SAR, which achieves higher spatial resolution, has contributed to the assessment of building damage induced by a tsunami disaster ([9], [10], [11]). A method for inspecting detailed damage to building side walls that is based on the side looking system in SAR observation has also been proposed for tsunami disasters ([12]).

These previously proposed approaches were based on change detection techniques using pre- and post-event SAR data. However, these methods cannot be applied in cases in which pre-event SAR data are not available. Therefore, a method that only requires post-event SAR data is necessary. Thus, the research question for this study is as follows: "What method can be used to detect damage in a building side wall using post-event SAR data?" A method for discriminating damage on building side walls was developed based on X-band polarimetric and interferometric airborne synthetic aperture radar (Pi-SAR2) full polarimetric data. The Pi-SAR2 system was developed by the National Institute of Information and Communications Technology (NICT). The building side walls in the areas affected by the 2011 Tohoku earthquake and tsunami were observed from four directions on the same day by the Pi-SAR2 platform. A building side wall shows bright backscattering induced by layover and double-bounce scattering. If the lower part of a building side wall is destroyed by a tsunami, double-bounce scattering, which is dominant in the lower part of a building side wall, may be absent and its scattering power may decrease. Considering this radar property in terms of building side walls, a method for identifying destroyed side walls was developed.

## 2. Data set and study area

The study area encompassed Sendai city, Miyagi Prefecture, Japan, which was affected by the 2011 Tohoku earthquake and tsunami. X-band full polarimetric airborne SAR data captured by the Pi-SAR2 platform were employed for damage detection. The observation was conducted on August 26, 2013 (JST), with four flight paths: 3, 4, 8 and 9. The spatial resolution ranged from 0.3-0.6 m in azimuth range and from 0.3-0.5 m in slant range. The Pauli color image of the Pi-SAR2 data in this study area and the path directions are shown in Fig. 1.

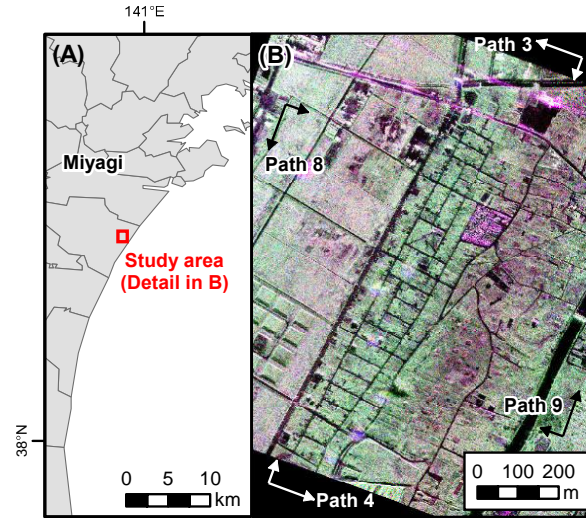


Fig. 1 (A) Study area and (B) Pauli color image with flight paths (R: HH-VV, G: HV, B: HH+VV)



Fig.2 Examples of destroyed and undestroyed building side walls: (A) destroyed and (B) undestroyed.

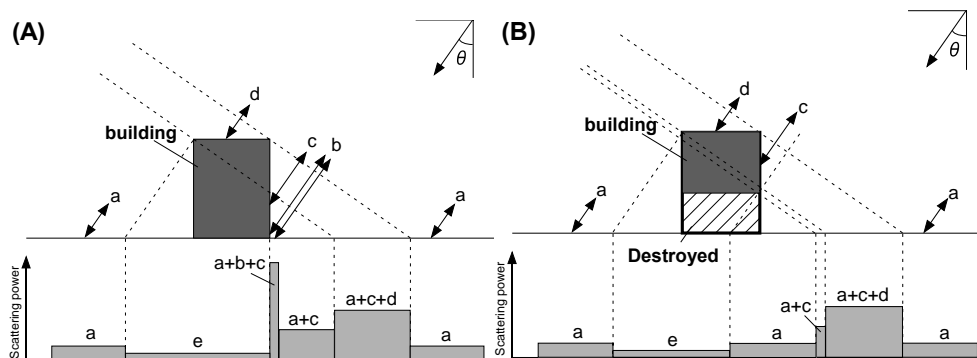


Fig.3 Radar properties on building geometries for the case of (A) a pre-tsunami event and (B) a post-tsunami event. Features of radar scatterings: a) surface scattering on the ground, b) double-bounce scattering, c) surface scattering on a building side wall, d) surface scattering on a roof, and e) radar shadow.

The incidence angles (near and far) for flight paths 3, 4, 8 and 9 were ( $35.4^\circ$  ,  $55.4^\circ$  ), ( $31.3^\circ$  ,  $52.3^\circ$  ), ( $29.3^\circ$  ,  $51.2^\circ$  ), ( $37.4^\circ$  ,  $55.4^\circ$  ), respectively.

The building footprint data were created based on the outline of the building roofs by a post-event World View-II image, which was captured on March 14, 2011 (UTC). Image processing of Pi-SAR2 data was conducted using PolSARpro software (ver. 4.2.0), distributed by the European Space Agency (ESA). 2.1 Numbering of subsections

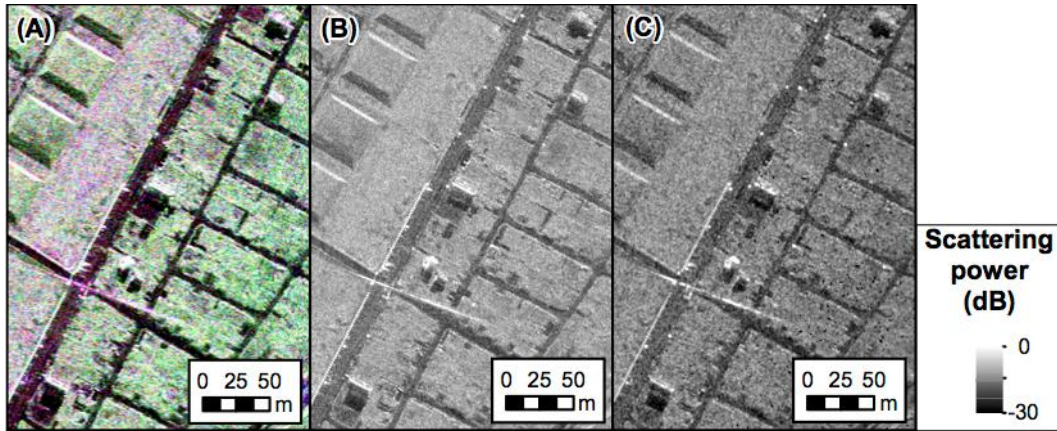


Fig.4 Examples of (A) Pauli color image (R: HH-VV, G: HV, and B: HH+VV), (B) total scattering power data and (C) double-bounce scattering power data.

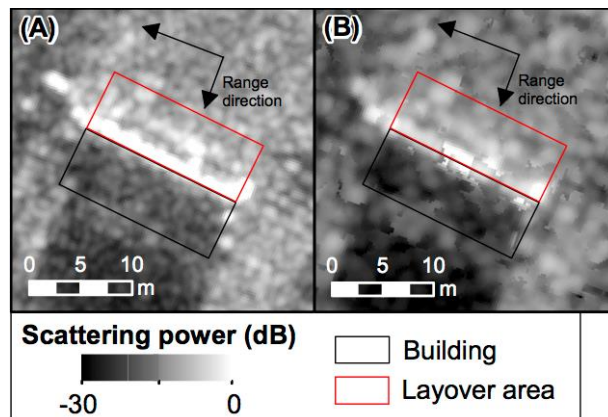


Fig.5 Building footprint and layover area with (A) total scattering power data and (B) double-bounce scattering data.

### 3. Damage detection

#### 3.1 Field survey and ground truth data

A field survey was conducted on August 13, 2013 (JST). A total of 12 buildings with 48 side walls were investigated, and building dimensions were measured in terms of building height, length, and corner coordinates. Then, building side walls were captured with a GPS camera. Example photos of building side walls are shown in Fig. 2. To classify “destroyed” and “undestroyed” buildings, damage levels were defined as follows:

- Destroyed: More than half of a building side wall on the first floor was destroyed (Fig. 2(A)).
- Undestroyed: Less than half of a building side wall on the first floor was destroyed (Fig. 2(B)).

#### 3.2 Radar properties of building geometry

Radar properties of buildings can be featured by bright and dark backscatters. A bright backscattering is induced by layover and double-bounce scattering, whereas a dark backscattering is induced by radar shadow. The geometries of radar backscatters to buildings are shown in Fig. 3. In an intact building, the scattering power on a building side wall that faces a radar beam yields a higher value due to layover and double-bounce scattering, as shown in Fig. 3(A).

If the first floor of a building is destroyed, double-bounce scattering may be absent and the scattering power in the layover area may decrease, as shown in Fig. 3 (B). The ratio of the double-bounce scattering power to the total scattering power in a layover area may decrease if the first floor of the building is destroyed by the tsunami.

### 3.3 Pre-processing

Complex data with amplitude and phase information in four polarizations (HH, HV, VH, and VV) were decomposed in terms of scattering matrix elements. The scattering matrix is expressed by the following equation:

$$S = \begin{bmatrix} S_{HH} & S_{HV} \\ S_{VH} & S_{VV} \end{bmatrix} = \begin{bmatrix} a & b \\ c & d \end{bmatrix} \quad (1)$$

where  $S_{HV}$  is the backscattering return from vertical transmitting and horizontal receiving polarizations. For simplicity,  $S_{HH}$ ,  $S_{VV}$  and  $S_{HV} \approx S_{VH}$  are represented by  $a$ ,  $b$  and  $c$ , respectively. Next, the scattering matrix was converted into a coherency matrix. The coherency matrix  $T$  is given by the following equation:

$$\langle T \rangle = \frac{1}{n} \sum k_p k_p^\dagger = \begin{bmatrix} T_{11} & T_{12} & T_{13} \\ T_{21} & T_{22} & T_{23} \\ T_{31} & T_{32} & T_{33} \end{bmatrix} \quad (2)$$

where  $T$  denotes complex conjugation and transposition,  $\langle \rangle$  denotes ensemble average, and the Pauli vector  $k_p$  is defined by the following equation:

$$k_p = \frac{1}{\sqrt{2}} \begin{bmatrix} a+b \\ a-b \\ 2c \end{bmatrix} \quad (3)$$

Gaussian Box Car filter with a window size of  $5 \times 5$  pixels was applied to obtain smoothed images with the edge information preserved.

Next, a four-component decomposition scheme was applied to expand the coherency matrix as follows:

$$\langle [T] \rangle^{HV} = f_s \langle [T] \rangle_{surf}^{hv} + f_d \langle [T] \rangle_{dbl}^{hv} + f_v \langle [T] \rangle_{vol}^{hv} + f_c \langle [T] \rangle_{hel}^{hv} \quad (4)$$

where  $f_s$ ,  $f_d$ ,  $f_v$  and  $f_c$  are the expansion coefficients and  $\langle [T] \rangle_{surf}^{hv}$ ,  $\langle [T] \rangle_{dbl}^{hv}$ ,  $\langle [T] \rangle_{vol}^{hv}$  and  $\langle [T] \rangle_{hel}^{hv}$  are the coherency matrices for surface scattering, double-bounce scattering, volume scattering and helix scattering, respectively ([13],[14]). The coherency matrix for double-bounce scattering is given by the following matrix:

$$[T]_{dbl}^{hv} = \begin{bmatrix} |\alpha|^2 & \alpha & 0 \\ \alpha^* & 1 & 0 \\ 0 & 0 & 0 \end{bmatrix} \quad (5)$$

where  $\alpha = (a+b)/(a-b)$  and  $|\alpha| < 1$  with the assumption that  $|a+b| < |a-b|$ . The variables  $a$ ,  $b$  and  $c$  were defined in Equation (1).

To detect building side walls destroyed by the tsunami, the total scattering power ( $TP$ ) was also utilized.  $TP$  is given by the following equation:

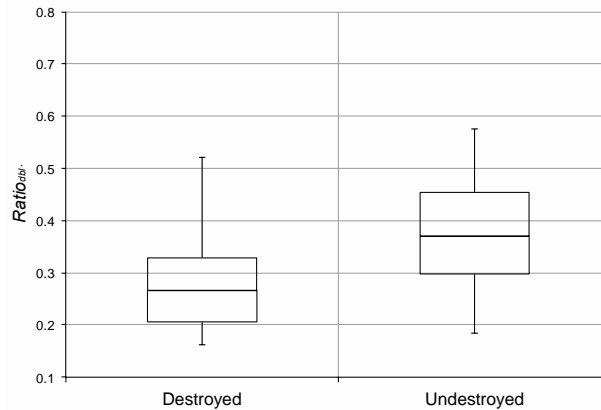


Fig.6 Boxplot of  $Ratio_{dbl}$  in terms of “destroyed” and “undestroyed” building side walls.

$$TP = 10 \log \left( \langle |a|^2 \rangle + 2 \langle |b|^2 \rangle + \langle |c|^2 \rangle \right) \quad (6)$$

Example images of the double-bounce scattering power and total scattering power with a Pauli color image are shown in Fig. 4.

### 3.4 Extracting the layover area

Using the building footprint data, the outline of the layover area in each building was extracted. The length of the layover area ( $L$ ) was calculated with the following equation:

$$L = H \cot \theta \quad (7)$$

where  $H$  is the height of the building and  $\theta$  is the incidence angle. The digital number of this layover area includes the scattering power from the building side wall. The building heights were measured in the field survey. An example of the extracted layover area is shown in Fig. 5. The layover areas for all building side walls were estimated based on the Pi-SAR2 data from each flight path.

### 3.5 Feature calculation

The ratio of the double-bounce scattering power to the total scattering power in the layover area ( $Ratio_{dbl}$ ) was calculated by the following equation:

$$Ratio_{dbl} = \frac{Pd}{TP} \quad (8)$$

where  $Pd$  is the double-bounce scattering power in the layover area and  $TP$  is the total scattering power in the layover area.

The values of  $Ratio_{dbl}$  were calculated for 48 building side walls of 12 buildings in the study area and correlated with the building damage (“destroyed” or “undestroyed”). The range of  $Ratio_{dbl}$  values according to damage levels was evaluated by creating box plots, as shown in Fig. 6.

According to this comparison, the 25th percentile and 75th percentile are represented by the bottom of the box and the top of the box ranges from 0.21 to 0.33 for “destroyed” and 0.30 to 0.45 for “undestroyed”, respectively. The distributions of these boxes reveal distinct differences, which

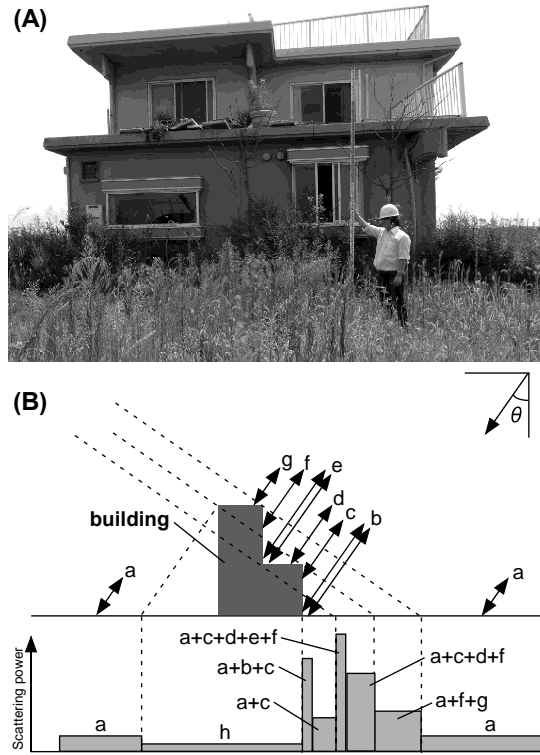


Fig.7 Buildings that induce double-bounce scattering on the second floor of the building. (A) An example photo and (B) radar properties of this structure: a) surface scattering on the ground, b) double-bounce scattering, c) surface scattering on a building side wall, d) surface scattering on the top of the first floor, e) double-bounce scattering on the second floor, f) surface scattering on a building sidewall, g) surface scattering on a roof, and h) radar shadow.

demonstrate the usefulness of  $Ratio_{dbl}$  for discriminating “destroyed” and “undestroyed” building side walls.

To determine the appropriate threshold value for  $Ratio_{dbl}$  to classify “destroyed” and “undestroyed” walls, a decision tree application of a machine learning algorithm was applied. To create the classifier C4.5, a decision tree application for binary classification, implemented on the data mining tool WEKA (ver. 3.6.9), was applied ([15],[16]). This tool is based on the concept of the Shannon entropy and is defined by the following equation:

$$i(N) = -\sum_j p(\omega_j) \log_2 p(\omega_j) \quad (9)$$

where  $N$  denotes the number of nodes,  $\omega_j$  is the name of the category and  $p(\omega_j)$  is the ratio of the number of patterns that belong to category  $\omega_j$ . A parameter and a threshold value for the classification were determined for each node to maximize the decrement of Shannon’s entropy using the following equation:

$$\Delta i(N) = i(N) - P_L i(N_L) - (1 - P_L) i(N_R) \quad (10)$$

where  $N_L$  and  $N_R$  are the children nodes of the left side and right sides, respectively, and  $P_L$  is the ratio of the number of patterns that relate to the left node. To create a robust and transferable tree, a 10-fold cross-validation was conducted. Specific variables on WEKA were established as follows: the

Table 1 – The results of building damage detection

		Classified result		
		Destroyed	Undestroyed	P.A. (%)
GTD	Destroyed	10	8	55.6
	Undestroyed	3	27	90.0
	U.A. (%)	76.9	77.1	Overall : 77.1

“confidence factor”, which is a variable related to post-pruning, was 0.25, and the “minimum number of objects” was 3.

#### 4. Results and discussion

A simple decision tree was obtained based on C4.5, the appropriate threshold value for discriminating between “destroyed” and “undestroyed” building side walls was determined to be 0.27. If  $Ratio_{dbl}$  is greater than 0.27, the wall was interpreted as “undestroyed”; otherwise, it was classified as “Destroyed”. The 48 building side walls were classified into “destroyed” and “undestroyed” based on the threshold value shown in TABLE I. The results show satisfactory performance, with 77.1 % total accuracy for classification with a kappa statistic of 0.48.

A comparison with the photos captured in the field survey indicated that the majority of the buildings with substantial damage to the wall yielded a lower  $Ratio_{dbl}$ . However, exceptions were noted: some buildings were destroyed by the tsunami, and some building side walls exhibited higher scattering power of double-bounce component. We investigated this finding and determined that walls in which double-bounce scattering was observed, such as balconies or other concavity and convexity, exhibited a trend of a higher double-bounce component in the scattering power. This finding was particularly evident in houses with a space on top of the first floor in addition to the second floor, which caused strong double-bounce scattering in the layover area, as shown in Fig. 7.

The primary improvement from previous studies is the proposition of a new method that does not require pre-event SAR data for the detection of destroyed walls. Thus, we are able to detect destroyed building side walls based on this method even if pre-event data is unavailable. Considering the situation of emergency response, it is practical to assume that pre-event SAR data will not be obtainable. Distinct criteria to discriminate destroyed walls can be proposed by ensuring high classification accuracy, which has not been proposed in previous approaches due to the limitations of spatial resolution and polarization. The proposed methods in this study are possible because of the very high resolution, up to 30 cm, and full polarimetric scattering data.

However, the transferability of this method should also be discussed. To ensure transferability, this method should be examined in the remaining test site. Forty-eight building side walls were analyzed, which is an insufficient sample size, and the method should be tested using a larger sample size. The model should also be verified using data with a different incidence angle. To develop a more robust method, these issues should be addressed in future studies.

## 5. Conclusion

This study proposed a method to detect tsunami-induced damage on building side walls using post-event polarimetric and interferometric airborne synthetic aperture radar (Pi-SAR2) full polarimetric data. Based on the assumption that double-bounce scattering, which is dominant in the lower part of a building side wall, decreases if the lower floor is destroyed by a tsunami, a new method for detecting the destroyed side wall of a building was developed. To extract the double-bounce scattering component from the total scattering power, a four-component decomposition scheme—the Yamaguchi decomposition—was applied using full polarimetric SAR data. The ratio of the double-bounce scattering power to the total scattering power in the layover area was calculated and correlated with the damage to the building side walls. A classifier to discriminate destroyed or undestroyed building side walls was created based on the decision tree application using the correlated data sets. The classifier demonstrated adequate performance for detecting damage on building side walls and yielded a total accuracy of 77.1 % and a kappa statistic of 0.48.

## 6. Acknowledgements

This research was financially supported by a Grant-in-Aid for Scientific Research (Project numbers: 25242035, 24241059), a Grant-in-Aid for JSPS Fellows (Project number:15H06107, 16K20988), and a CREST project grant (Project manager : Shunichi Koshimura). We received the Pi-SAR2 data from NICT as a collaborative project.

## 7. Copyrights

16WCEE-IAEE 2016 reserves the copyright for the published proceedings. Authors will have the right to use content of the published paper in part or in full for their own work. Authors who use previously published data and illustrations must acknowledge the source in the figure captions.

## 8. References

- [1] The 2011 Tohoku Earthquake Tsunami Joint Survey Group, <http://www.coastal.jp/tsunami2011/>, referred on October 2013
- [2] National Police Agency, Report of the damage caused by the 2011 Tohoku earthquake and tsunami (in Japanese), <http://www.npa.go.jp/archive/keibi/biki/higaijokyo.pdf>, referred on October 2013
- [3] S.Koshimura, S.Hayashi and H.Gokon, Lessons of the 2011 Tohoku Earthquake Tsunami Disaster, *Journal of Disaster Research*, Vol.8, No.4 pp. 549-560, 2013
- [4] F.Dell'Acqua and P.Gamba, Remote sensing and earthquake damage assessment: experiences, limits, and perspectives, *Proceedings of the IEEE*, Vol. 100, No. 10, October 2012
- [5] M.Matsuoka and F.Yamazaki, Use of satellite SAR intensity imagery for detecting building areas damaged due to earthquakes, *Earthquake Spectra*, Vol. 20, No. 3, pp. 975-994, 2004
- [6] M.Matsuoka and M.Estrada, Development of Earthquake-induced Building Damage Estimation Model Based on ALOS/PALSAR Observing the 2007 Peru Earthquake, *Journal of Disaster Research*, Vol.8, No.2, pp.346-355, 2013
- [7] D.Brunner, G.Lemoine and L.Bruzzozone, Earthquake damage assessment of buildings using VHR optical and SAR imagery, *IEEE Transactions on Geoscience and Remote Sensing*, Vol. 48, No. 5, May 2010
- [8] W.Liu, F.Yamazaki, H.Gokon and S.Koshimura, Extraction of tsunami-flooded areas and damaged buildings in the 2011 Tohoku-oki earthquake from TerraSAR-X intensity images, *Earthquake Spectra*, Vol. 29, No. S1, pages S183-S200, March 2013
- [9] S.Chen and M.Sato, Tsunami damage investigation of built-up areas using multitemporal spaceborne full polarimetric SAR images, *IEEE Transactions on Geoscience and Remote Sensing*, Vol. 51, No. 4, April 2013
- [10] M.Sato, S.Chen and M.Satake, Polarimetric SAR analysis of tsunami damage following the March 11, 2011 east Japan earthquake, *Proceedings of the IEEE*, Vol. 100, No. 10, October 2012

- [11] M.Watanabe, T.Motohka, Y.Miyagi, C.Yonezawa and M.Shimada, Analysis of urban areas affected by the 2011 off the paacific coast of Tohoku earthquake and tsunami with L-Band SAR full-polarimetric mode, *IEEE Geoscience and Remote Sensing Letters*, Vol.9, No.3, May 2012
- [12] F.Yamasaki, Y.Iwasaki, W.Liu, T.Nonaka and T.Sasagawa, Detection of damage to building side walls in the 2011 Tohoku, Japan earthquake using high-resolution TerraSAR-X images, Images, *SPIE 8892, Image and Signal Processing for Remote Sensing XIX*, 889212, 2013
- [13] Y.Yamaguchi, T.Moriyama, M.Ishido and H.Yamada, Four-Component Scattering Model for Polarimetric SAR Image Decomposition, *IEEE Transactions on Geoscience and Remote Sensing*, Vol. 43, No. 8, August 2005
- [14] Y.Yamaguchi, Y.Yajima and H.Yamada, A Four-Component Decomposition of POLSAR Images Based in the Coherency Matrix, *IEEE Geoscience and Remote Sensing Letters*, Vol. 3, No. 3, July 2006
- [15] J.R.Quinlan, C4.5: Programs for machine learning. San Mateo, Calif.: Morgan Kaufmann, 1993.
- [16]M.Hall, E.Frank, G.Holmes, B.Pfahring, P.Reutemann and I.H.Witten, The WEKA Data Mining Software: An Update; *SIGKDD Explorations*, Volume 11, Issue 1, 2009